REDUCED MODELS FOR THICK LIQUID LAYERS WITH INERTIA ON HIGHLY CURVED SUBSTRATES

ALEXANDER W. WRAY , DEMETRIOS T. PAPAGEORGIOU , AND OMAR K. MATAR

Abstract. A method is presented for deriving reduced models for fluid flows over highly curved substrates with wider applicability and accuracy than existing models in the literature. This is done by reducing the Navier-Stokes equations to a novel system of boundary layer like equations in a general geometric setting. This is accomplished using a new, relaxed set of scalings that assert only that streamwise variations are 'slow'. These equations are then solved using the method of weighted residuals, which is demonstrated to be applicable regardless of the geometry selected. A large number of results in the literature can be derived as special cases of our general formulation. A few of the more interesting cases are demonstrated. Finally, the formulation is applied to two thick annular flow systems as well as a conical system in both linear and nonlinear regimes, which traditionally has been considered inaccessible to such reduced models. Comparisons are made with direct numerical simulations of the Stokes equations. The results indicate that reduced models can now be used to model systems involving thick liquid layers.

Key words.

1. Introduction. Film flows have been the subject of multiple major reviews [31, 11, 8] due to their fundamental significance in a wide variety of contexts. For example, they are critical to our understanding of many physical processes, such as avalanches [2], ice sheet models [3], in underwater and lava flows [19, 20], tear films on the surface of an eye [44, 51, 6] and the well-known 'coffee-stain' effect [12]. They are also of central importance in many industrial applications such as heat and mass transfer as well as in a wealth of micro-[48, 47] and nanotechnological settings [13].

As a result, it is unsurprising that considerable attention and study has been given to reduced models, which greatly simplify the governing equations yet retain an accurate description of the physics of the system. The idea is to reduce the dimensionality of the problem by one through weighted integration over the thickness. It is not possible to do this for the general form of the Navier-Stokes equations, and thus a common (although not universal) approach is to exploit some disparity in length scales in the problem in order to reduce the Navier-Stokes equations to some simpler, solvable system. In general, we define some 'small' parameter ϵ sometimes known as an aspect ratio, slenderness parameter or lubrication parameter depending on the context. In the case of planar flows, this is typically defined as $\epsilon = H/L$ where H is some characteristic length scale in the cross-stream direction (often the thickness) and L is a characteristic length scale in the streamwise direction (often a characteristic wavelength). This is therefore often known as a *long-wave* or *thin-film* expansion.

In a planar geometry the terms "long-wave" and "thin-film" are used essentially interchangeably as the only length scales in the problem are the thickness of the liquid layer and the length of the waves. Considering the former to be small is equivalent to assuming the latter to be large. However, working on a curved substrate introduces two additional length scales, namely the two principal radii of curvature of the substrate. We therefore use the following two conventions rigorously throughout:

1. In a *thin-film* approximation, wavelengths are assumed to be $\mathcal{O}(1)$, as are radii of curvature (or infinite and thus irrelevant), while the film thickness is assumed to be 'small' (typically of $\mathcal{O}(\epsilon)$).
2. In a *long-wave* approximation, wavelengths are assumed to be 'long' (typically $\mathcal{O}\left(\epsilon^{-1}\right)$), while the radii of curvature and the film thickness are assumed to be $\mathcal{O}(1)$.

Over time, successively more sophisticated methods have been applied to the development of reduced models in order to improve their accuracy and breadth of applicability. This began with the investigations of Benjamin [4] and Yih [54] who applied a thin-film approximation followed by a linearisation procedure in order to investigate the linear behaviour of falling films on inclined planes. This thin-film procedure has also famously been applied in a nonlinear context by Benney [5] to planar flows, and by Hammond [15] to core-annular flows to derive nonlinear evolution equations for the interface. Benney's equation retains the effects of inertia but, unfortunately, is known to suffer from unphysical blowup [33, 22] when the Reynolds number is sufficiently large. The exact value depends on the Kapitza number and the inclination angle, but is typically of order unity [41].

Weakly nonlinear theory has also been applied to derive an interfacial evolution equation that is valid even in the presence of inertia [46]. However, this relies on the assumption that the magnitude of the deviation of the interface from the basic state is small relative to the thickness of the layer, and as a result is only applicable close to threshold.

Attempts to allow for the incorporation of inertia have been made by Kaptiza & Kapitza [23] and Shkadov [45] using a Kármán-Pohlhausen technique. Unfortunately however, while this cures the unphysical blowup of Benney's equation, the resultant evolution equations do not correctly predict the onset of linear instability, and as a result may not be acceptable as model equations. This was resolved by the weighted residual integral boundary layer (WRIBL) method described by Ruyer-Quil et al. [38]. The method is essentially a separation of variables, Galerkin-type approach which results in coupled equations for the interfacial position and the local flux and allows for moderate levels of inertia whilst correctly predicting the linear onset of instabilities and not exhibiting finite time blowup.

Many of these approaches have been applied to flows down wavy inclines. Aksel and collaborators have subjected such flows to extensive analysis via experiments [49], direct numerical simulations [42] and order reducing modelling using both typical asymptotic expansions [50], and a Kármán-Pohlhausen method [16]. Incidentally, while the substrate is no longer flat, the underlying geometry is still typically cartesian. Instead, all conditions at the wall are simply applied at some spatially varying normal co-ordinate corresponding to the wall position. The experiments and numerical simulations revealed vortex structures in deep undulations which have since been recovered qualitatively using a weighted residual formulation [32].

In addition to the canonical geometries such as the cartesian and core-annular situations described above, lubrication theory has also been applied to systems of arbitrary curved surfaces. Such analyses typically proceed by using curvilinear co-ordinates relative to the underlying substrate. The fundamental geometry and equations were originally introduced by Howell [17] in the context of three-dimensional thin viscous sheets. The same methodology was used by Roy et al. [37] for thin-film flow over fixed substrates. At leading order this gives rise to capillarity driven flow, while at higher orders centre manifold theory was used to derive more complicated equations incorporating the effect of inertia. The resultant model was then applied to a variety of geometries including flow over the outside of a corner, and on the surface of a torus. This model was subsequently extended, for example by Roberts & Li [35] to incorporate higher levels of inertia, and by Howell [18] to incorporate moving surfaces.

Geometrically speaking, however, almost all studies in non-planar geometries have

confined themselves to the thin-film approximation, so that locally the system looks quasi-planar [35, 37, 15, 32, 27, 28, 34]. The only exceptions require some other restrictive assumption in order to make analytical progress, such as the imposition of axisymmetry in a fibre context [10, 39]. However, this means that a wealth of interesting phenomena are challenging to access with such reduced models. For example, Kalliadasis & Chang [21] point out that fibre flows will exhibit non-axisymmetric instabilities at appropriate Reynolds numbers when the film is sufficiently thick. However, at the moment this has only been accessible in a weakly-nonlinear regime [46] that does not correspond to experimental observations. In order to perform fully nonlinear calculations the only option appears to be direct numerical simulations. Indeed, even in the simpler two-dimensional case of a liquid layer hanging from a horizontal cylinder, modellers have previously been confined to using a thin-film approximation outside its range of validity [7]. This can push the asymptotic approximation too far. In Section 5 we give an example of an annular ring of fluid decaying under the effect of surface tension. When the thickness is equal to half the radius of the cylinder and for an azimuthal disturbance of wavenumber 6, linearised lubrication theory is in error by over 1400%, as opposed to less than 6% for the new theory presented.

Most models have not been designed to be applicable to the situation where the radius of curvature of the substrate and the thickness of the film are comparable. We give a formulation that attempts to resolve this problem. The key points of the method that we use are as follows:

1. We use the geometry described by Roberts & Li [35] as detailed in Section 2.2.
2. In order to overcome some of the limitations inherent in the geometry described by Roberts & Li we allow the substrate to be located at $y = \zeta$ where ζ is a function of space.
3. We use a novel set of 'long-wave' scalings in Section 3.1 to reduce the governing equations to a general set of boundary layer equations.
4. We retain the full form of the curvature term as suggested by Rosenau et al. [36]; a commonly used approach when fluid layers are thick [24]. This retains terms of higher order than the rest of the derivation. If so desired for consistency, this can be remedied by selecting an appropriately truncated expression for the curvature.
5. We then apply a separation of variables approach, using the method of weighted residuals but projecting only onto the leading order polynomial as suggested by Scheid et al. [40], in order to derive a reduced model.

We demonstrate the general nature of our formulation in Section 4 by recovering a number of existing models in the literature. We then demonstrate the high degree of accuracy of our formulation even in thick liquid layers on highly curved substrates with three case studies: in Section 5 we compare the linearisation of thin-film and long-wave models for thick annular flow around a disc to the results of exact linear theory; in Section 6 we give a nonlinear comparison for thin-film and long-wave models against direct numerical simulations for a thick film hanging from a spinning horizontal cylinder; in Section 7 we compare nonlinear calculations for flow over the surface of a cone to the predictions of direct numerical simulations. In all cases the long-wave model performs well. However, with the exception of §4.3 at $Re = 1$ the model has only been tested in the absence of inertia. Finally, in Section 8 we give our conclusions.

2. Problem formulation. We describe the flow of a layer of liquid over an arbitrary surface, incorporating the effects of viscosity, capillarity, gravity and inertia.

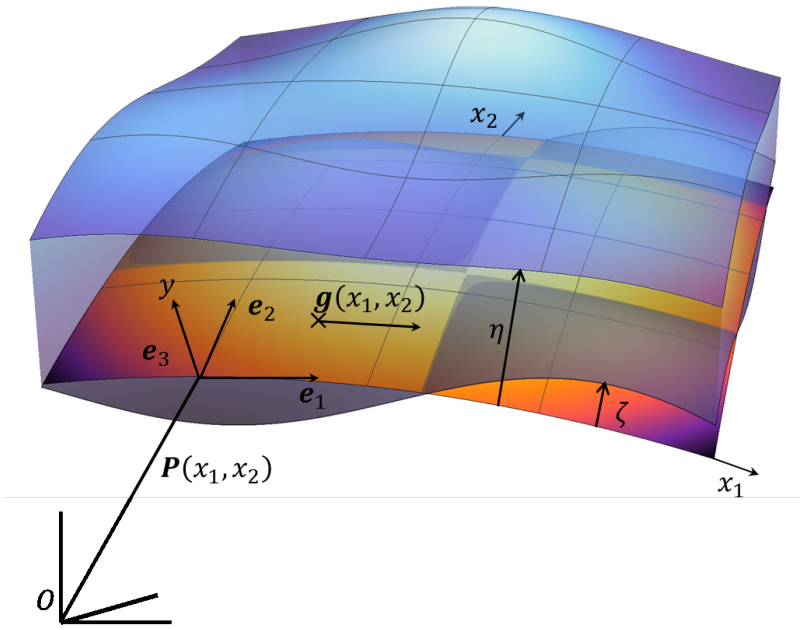

FIG. 1. *A schematic of the situation being considered: relative to an reference surface* $\mathbf{P}$*, a liquid rests on a curved surface* $y = \zeta$ *with the interface lying at* $y = \eta$*.*

We give a schematic of the geometry in Figure 1. We begin by giving the equations governing the system in co-ordinate free form in Section 2.1. We then describe the body-mapped geometry system we are using in Section 2.2 and give the Navier-Stokes equations in this co-ordinate system.

2.1. Governing equations. The fluid is taken to have constant density ρ, velocity $\mathbf{u}$, pressure p, dynamic viscosity μ with the gravity denoted by $\mathbf{g}$. We non-dimensionalise lengths using the typical film thickness H, and introduce

$$\mathbf{u} = U\tilde{\mathbf{u}}, \quad p = \frac{U\mu}{H}\tilde{p}, \quad t = \frac{H}{U}\tilde{t}, \tag{2.1}$$

where $U = \frac{\rho g H^2}{\mu}$ is a characteristic velocity. In the absence of gravity (see Section 5) or when the substrate is flat and the gravity is normal to it, we use $U = \gamma/\mu$. Dropping tilde decorations, the dimensionless momentum and continuity equations are respectively

$$Re\frac{D\mathbf{u}}{Dt} = \nabla \cdot \mathbf{T} + \mathbf{g}, \quad \nabla \cdot \mathbf{u} = 0, \tag{2.2}$$

where $Re = \frac{\rho U H}{\mu}$ is the Reynolds number, $\mathbf{T} = -p\mathbf{I} + \tau$ is the total stress tensor and τ is the usual Cauchy stress tensor. This is to be solved subject to no-slip on the substrate, and the appropriate stress conditions at the interface:

$$[\mathbf{n} \cdot \mathbf{T} \cdot \mathbf{n}] = \frac{\kappa}{Ca}, \quad [\mathbf{n} \cdot \mathbf{T} \cdot \mathbf{t}_i] = 0, \tag{2.3}$$

where $\mathbf{n}$ is the normal vector to the surface, $\mathbf{t}_i, i = 1, 2$ are two tangential vectors to the surface, given explicitly shortly, $Ca = \frac{U\mu}{\gamma}$ is the Capillary number, which determines the relative significance of viscous effects compared to surface tension, and $[\cdot]$ represents the jump in the value of a quantity across the interface.

2.2. Geometry and transformed equations. We give a brief outline of the orthogonal co-ordinate system shown schematically in Figure 1; for more details see Roy et al., [37], Roberts & Li [35] and Miksis & Ida [27]. Consider the reference surface P parametrized by the two co-ordinates x_1 and x_2, with unit vectors $\mathbf{e}_1$ and $\mathbf{e}_2$ corresponding to $x_2 =$ constant and $x_1 =$ constant respectively. While this prescribes the geometry in which our system resides, this need not be the surface of the substrate itself: for example imagine describing a golf ball with dimples. P would most easily be given as the surface of a sphere, with the dimples being prescribed by locating the substrate at a spatially varying value of y as described shortly. The unit normal to the reference surface is denoted by $\mathbf{e}_3$, with y measuring the distance in this direction such that $\mathbf{e}_1$, $\mathbf{e}_2$ and $\mathbf{e}_3$ form a right-handed set of locally orthogonal co-ordinate vectors. The interface is located at $y = \eta$. In this co-ordinate system the x_1, x_2 and y components of velocity and gravity are $\mathbf{u} = (u_1, u_2, v)$ and $\mathbf{g} = (g_1, g_2, g_3)$. Due to the curvature of the substrate, gravity generally depends on x_1 and x_2. The reference surface P is given in space as $\mathbf{x} = \mathbf{P}(x_1, x_2)$, relative to which any point in the fluid can be expressed as

$$\mathbf{X}(x_1, x_2, y) = \mathbf{P}(x_1, x_2) + y\mathbf{e}_3(x_1, x_2), \tag{2.4}$$

so long as $\eta(x_1, x_2)$ is less than the principal curvature in each direction, when that curvature is positive so that the surface is concave; otherwise the geometry is ill-defined [37]. This excludes the potential to examine certain regimes, such as flow over a step. In order to circumvent this issue and access a wider array of flow scenarios the substrate is located at $y = \zeta(x_1, x_2)$, which must obey the same constraints as η. This is in contrast to Roy et al. [37] and Roberts & Li [35] who effectively enforced $\zeta = 0$. The no-slip and impermeability conditions are then expressed on $y = \zeta$ as

$$u_1 = u_2 = v = 0. \tag{2.5}$$

On the substrate $\mathbf{e}_i = \frac{1}{m_i}\frac{\partial \mathbf{P}}{\partial x_i}$ for $i = 1, 2$, where $m_i = \left|\frac{\partial \mathbf{P}}{\partial x_i}\right|$ are the metric scale factors. In addition $\frac{\partial \mathbf{e}_3}{\partial x_i} = -m_i k_i \mathbf{e}_i$, where k_i are the corresponding principal curvatures of the substrate. At any point $\mathbf{X}$ in the fluid, the scale factors of the spatial coordinate system are

$$h_i = \left|\frac{\partial \mathbf{X}}{\partial x_i}\right| = m_i(1 - k_i y), \quad h_3 = \left|\frac{\partial \mathbf{X}}{\partial y}\right| = 1. \tag{2.6}$$

We need the appropriate derivatives of the unit vectors. As given by Roberts & Li [35],

$$\frac{\partial \mathbf{e}_i}{\partial x_i} = -\frac{1}{h_i'}\frac{\partial h_i}{\partial x_{i'}}\mathbf{e}_{i'} + m_i k_i \mathbf{e}_3, \quad \frac{\partial \mathbf{e}_i}{\partial y} = \frac{\partial \mathbf{e}_3}{\partial y} = \mathbf{0}, \tag{2.7}$$

$$\frac{\partial \mathbf{e}_3}{\partial x_i} = -m_i k_i \mathbf{e}_i, \quad \frac{\partial \mathbf{e}_i}{\partial x_{i'}} = \frac{1}{h_i}\frac{\partial h_{i'}}{\partial x_i}\mathbf{e}_{i'}, \tag{2.8}$$

where $i = 1, 2$ and $i' = 3-i$. We also require an expression for the interfacial curvature to determine the effects of capillarity. In this geometry it is [35]
(2.9)

$$\kappa = \frac{1}{\tilde{h}_1\tilde{h}_2}\left[\frac{\partial}{\partial x_1}\left(\frac{\tilde{h}_2^2\eta_{x_1}}{\mathscr{A}}\right) + \frac{\partial}{\partial x_2}\left(\frac{\tilde{h}_1^2\eta_{x_2}}{\mathscr{A}}\right)\right] + \frac{1}{\mathscr{A}}\left[\left(\tilde{h}_1^2 + \eta_{x_1}^2\right)\frac{m_2k_2}{\tilde{h}_1} + \left(\tilde{h}_2^2 + \eta_{x_2}^2\right)\frac{m_1k_1}{\tilde{h}_2}\right],$$

where $\tilde{h}_i = h_i|_{y=\eta} = m_i\left(1 - k_i\eta\right)$ are the metric coefficients evaluated at the interface, and

$$\mathscr{A} = \sqrt{\tilde{h}_1^2\tilde{h}_2^2 + \tilde{h}_2^2\eta_{x_1}^2 + \tilde{h}_1^2\eta_{x_2}^2}. \tag{2.10}$$

The normal and tangent vectors to the interface $\tilde{\mathbf{X}} = \mathbf{X}|_{y=\eta}$ are given by Roberts & Li [35] (18)-(19)

$$\tilde{\mathbf{t}}_i = \frac{\partial\tilde{\mathbf{X}}}{\partial x_i}\Bigg/\left|\frac{\partial\tilde{\mathbf{X}}}{\partial x_i}\right| = \left(\tilde{h}_i\mathbf{e}_i + \eta_{x_i}\mathbf{e}_3\right)/\sqrt{\tilde{h}_i^2 + \eta_{x_i}^2}, \tag{2.11}$$

$$\tilde{\mathbf{n}} = \frac{\tilde{\mathbf{t}}_1 \times \tilde{\mathbf{t}}_2}{\left|\tilde{\mathbf{t}}_1 \times \tilde{\mathbf{t}}_2\right|} = \left(-\tilde{h}_2\eta_{x_1}\mathbf{e}_1 - \tilde{h}_1\eta_{x_2}\mathbf{e}_2 + \tilde{h}_1\tilde{h}_2\mathbf{e}_3\right)/\mathscr{A}. \tag{2.12}$$

The Navier-Stokes equations (2.2) become [35] (25)

$$\begin{aligned} Re\Bigg\{&\frac{\partial\mathbf{u}}{\partial t} + \mathbf{e}_1\left[\mathbf{u}\cdot\nabla u_1 + \frac{u_2}{h_1h_2}\left(u_1\frac{\partial h_1}{\partial x_2} - u_2\frac{\partial h_2}{\partial x_1}\right) - m_1k_1\frac{vu_1}{h_1}\right] \\ &+ \mathbf{e}_2\left[\mathbf{u}\cdot\nabla u_2 + \frac{u_1}{h_1h_2}\left(u_2\frac{\partial h_2}{\partial x_1} - u_1\frac{\partial h_1}{\partial x_2}\right) - m_2k_2\frac{vu_2}{h_2}\right] \\ &+\mathbf{e}_3\left[\mathbf{u}\cdot\nabla v + m_1k_1\frac{u_1^2}{h_1} + m_2k_2\frac{u_2^2}{h_2}\right]\Bigg\} = -\nabla p - \nabla\times\boldsymbol{\omega} + \mathbf{g}, \end{aligned} \tag{2.13}$$

where $\mathbf{u}\cdot\nabla = \frac{u_1}{h_1}\frac{\partial}{\partial x_1} + \frac{u_2}{h_2}\frac{\partial}{\partial x_2} + v\frac{\partial}{\partial y}$, and $\boldsymbol{\omega}$ is the vorticity of the fluid, defined by

$$\boldsymbol{\omega} = \nabla\times\mathbf{u} = \frac{\mathbf{e}_1}{h_2}\left[\frac{\partial v}{\partial v_2} - \frac{\partial\left(h_2u_2\right)}{\partial y}\right] + \frac{\mathbf{e}_2}{h_1}\left[\frac{\partial\left(h_2u_1\right)}{\partial y} - \frac{\partial v}{\partial x_1}\right] \tag{2.14}$$

$$+ \frac{\mathbf{e}_2}{h_1h_2}\left[\frac{\partial\left(h_2u_2\right)}{\partial x_1} - \frac{\partial\left(h_1u_1\right)}{\partial x_2}\right]. \tag{2.15}$$

We have also used $\nabla\cdot\mathbf{u} = 0$ (2.2), which in this co-ordinate system is

$$\frac{\partial}{\partial x_1}\left(h_2u_1\right) + \frac{\partial}{\partial x_2}\left(h_1u_2\right) + \frac{\partial}{\partial y}\left(h_1h_2v\right) = 0. \tag{2.16}$$

The kinematic condition $\frac{D}{Dt}\left(y - \eta\right) = 0$ expands as [35] (27)

$$\frac{\partial\eta}{\partial t} = v - \frac{u_1}{\tilde{h}_1}\frac{\partial\eta}{\partial x_1} - \frac{u_2}{\tilde{h}_2}\frac{\partial\eta}{\partial x_2} \tag{2.17}$$

at $y = \eta$. Finally, the components of the Cauchy stress tensor become [35] (30)

$$\tau_{ii} = 2\left(\frac{1}{h_i}\frac{\partial u_i}{\partial x_i} + \frac{u_{i'}}{h_ih_{i'}}\frac{\partial h_i}{\partial x_{i'}} - \frac{m_ik_i}{h_i}v\right), \quad \tau_{33} = 2\frac{\partial v}{\partial y}, \tag{2.18}$$

$$\tau_{12} = \frac{1}{h_2}\frac{\partial u_1}{\partial x_2} + \frac{1}{h_1}\frac{\partial u_2}{\partial x_1} - \frac{u_1}{h_1h_2}\frac{\partial h_1}{\partial x_2} - \frac{u_2}{h_1h_2}\frac{\partial h_2}{\partial x_1}, \tag{2.19}$$

$$\tau_{i3} = \frac{1}{h_i}\frac{\partial v}{\partial x_i} + \frac{\partial u_i}{\partial y} + \frac{m_ik_i}{h_i}u_i. \tag{2.20}$$

3. Reduced models. In order to make analytical progress we begin by applying a long-wave approximation in Section 3.1 to derive a boundary layer type set of equations. We solve these to first order in absence of inertia in Section 3.2, and then use a variation of the method of weighted residuals to give an integral formulation for such models at higher orders in Section 3.3.

3.1. Boundary layer equations. We invoke a novel long-wave assumption in order to derive a reduced set of boundary layer equations in this generalised geometry setting. Assume that the characteristic length of structures in the streamwise direction is 'long' relative to the thickness of the film, i.e. $\partial_{x_i} \mapsto \epsilon\,\partial_{x_i}$ (including film structures as well as the gradients of the curvatures and the substrate position ζ).

ϵ is to be treated as an "ordering parameter" [40]: that is, it serves only to assert the anticipated relative magnitudes of terms during calculation and is taken to be unity in the final model. Secondly, unlike Roy et al. [37] and Roberts & Li [35], we do *not* make any scaling assumptions on the magnitude of the curvatures k_i (though their derivatives must still be of order ϵ). At the cost of slightly complicating the analysis, this retains some greater generality than either of those papers; as a result we recover models that they cannot, such as that of Craster & Matar [10] (§4.1). We also show (§5) that it aids in the accuracy of modelling thick films.

We are assuming that our substrates have $\mathcal{O}(1)$ curvatures. It might reasonably be expected that this could induce flow structures with characteristic wavelength of $\mathcal{O}(1)$; this stands to violate the assumption that waves are 'long'. As a result comparison and validation must be performed *a posteriori*; in practice we show via validation against full linear theory and direct numerical simulations that the long-wave assumption provides good results outside its strict realms of anticipated applicability. Roberts & Li [35] showed that in their context the long-wave expansion was valid provided that the relative gradients for any quantity w satisfy $\left|\frac{\nabla w}{w}\right| < \frac{1.9}{\eta}$.

We make the long-wave substitutions $x_i = \hat{x}_i/\epsilon$, where all quantities with hats are of order unity. A scaling argument using the continuity equation (2.16) shows that $v = \mathcal{O}(\epsilon)$, so we assert this by incorporating an appropriate instance of the ordering parameter by making the substitution $v = \epsilon\hat{v}$. Similarly, the kinematic condition (2.17) suggests taking $t = \hat{t}/\epsilon$. The hat decoration is then dropped. Integrating (2.16) from the substrate to the interface and substituting into (2.17) gives

$$\tilde{h}_1\tilde{h}_2\frac{\partial\eta}{\partial t} + \begin{pmatrix}\partial_{x_1}\\ \partial_{x_2}\end{pmatrix}\cdot\int_\zeta^\eta \begin{pmatrix}h_2u_1\\ h_1u_2\end{pmatrix}\,dy = 0. \tag{3.1}$$

To derive the boundary layer equations, we first calculate an expression for the pressure by applying the long-wave scalings to the $\mathbf{e}_3$ component of (2.13) to find

$$\begin{aligned}\frac{\partial p}{\partial y} = g_3 - Re\left(m_1k_1\frac{u_1^2}{h_1} + m_2k_2\frac{u_2^2}{h_2}\right)\\ - \frac{\epsilon}{h_1h_2}\left[\frac{\partial}{\partial x_1}\left(\frac{h_2}{h_1}\frac{\partial\left(h_1u_1\right)}{\partial y}\right) + \frac{\partial}{\partial x_2}\left(\frac{h_1}{h_2}\frac{\partial\left(h_2u_2\right)}{\partial y}\right)\right] + \mathcal{O}\left(\epsilon^2\right).\end{aligned} \tag{3.2}$$

As p only appears at first order in the x_1 and x_2 components of the momentum equation, this first order expression is sufficient for a second order expression for the velocities u_i. Expanding $\mathbf{t}_i\cdot\mathbf{T}\cdot\mathbf{n} = 0$ explicitly tells us that $\tau_{i3} = \mathcal{O}(\epsilon)$. Therefore we discard the second order terms of the form $\eta_{x_i}\tau_{i3}$ in the long-wave expansion of

the normal stress condition (2.3) so that

$$p|_{y=\eta} = \frac{\kappa}{Ca} + \epsilon\, 2\, \frac{\partial v}{\partial y}\bigg|_{y=\eta} + \mathcal{O}\left(\epsilon^2\right). \tag{3.3}$$

Integrating (3.2) from y to η using this stress condition, and where κ/Ca is assumed order unity, yields

$$\begin{aligned} p = {} & g_3\left(y-\eta\right) + \frac{\kappa}{Ca} + Re\, K_I\left(x_1, x_2, y\right) \\ & + \epsilon \left\{ \left[\frac{1}{h_1 h_2} \frac{\partial \left(h_1 h_2 v\right)}{\partial y} \right]_{\eta}^{y} + 2\, \frac{\partial v}{\partial y}\bigg|_{y=\eta} + K_V\left(x_1, x_2, y\right) \right\} + \mathcal{O}\left(\epsilon^2\right), \end{aligned} \tag{3.4}$$

where $K_{I,V}$ are

$$K_I = \int_y^{\eta} \left(m_1 k_1 \frac{u_1^2}{h_1} + m_2 k_2 \frac{u_2^2}{h_2} \right) dy, \tag{3.5}$$

$$\begin{aligned} K_V = \int_y^{\eta} \frac{1}{h_1 h_2} & \left[\frac{\partial}{\partial x_1} \left(u_1 h_1 \frac{\partial}{\partial y} \left(\frac{h_2}{h_1} \right) \right) + \frac{\partial}{\partial x_2} \left(u_2 h_2 \frac{\partial}{\partial y} \left(\frac{h_1}{h_2} \right) \right) \right] \\ & - \frac{\partial}{\partial y} \left(\frac{1}{h_1 h_2} \right) \frac{\partial (h_1 h_2 v)}{\partial y} dy. \end{aligned} \tag{3.6}$$

Expansion of (2.13) yields the desired boundary layer equations. The resultant equation for u_1 is

$$\begin{aligned} & \epsilon Re \left\{ \frac{\partial u_1}{\partial t} + \frac{u_1}{h_1}\frac{\partial u_1}{\partial x_1} + \frac{u_2}{h_2}\frac{\partial u_1}{\partial x_2} + v\frac{\partial u_1}{\partial y} + \frac{u_2}{h_1 h_2}\left(u_1 \frac{\partial h_1}{\partial x_2} - u_2 \frac{\partial h_2}{\partial x_1} \right) - m_1 k_1 \frac{v u_1}{h_1} \right\} \\ & + \frac{\epsilon}{h_1}\frac{\partial p}{\partial x_1} - g_1\left(x_1, x_2\right) = \\ & \quad \frac{1}{h_2}\frac{\partial}{\partial y}\left(\frac{h_2}{h_1}\frac{\partial}{\partial y}\left(h_1 u_1\right) \right) + \epsilon^2 \frac{1}{h_1}\frac{\partial}{\partial x_1}\left(\frac{1}{h_1 h_2}\frac{\partial}{\partial x_1}\left(h_2 u_1\right) \right) + \epsilon^2 \frac{1}{h_2}\frac{\partial}{\partial x_2}\left(\frac{1}{h_1 h_2}\frac{\partial}{\partial x_2}\left(h_1 u_1\right) \right) \\ & \quad + \epsilon^2 \left[\frac{1}{h_1}\frac{\partial}{\partial x_1}\left(\frac{1}{h_1 h_2}\frac{\partial \left(h_1 u_2\right)}{\partial x_2} \right) - \frac{1}{h_2}\frac{\partial}{\partial x_2}\left(\frac{1}{h_1 h_2}\frac{\partial \left(h_2 u_2\right)}{\partial x_1} \right) \right] \\ & \quad + \epsilon^2 \left[\frac{1}{h_1}\frac{\partial}{\partial x_1}\left(\frac{v}{h_1 h_2}\frac{\partial \left(h_1 h_2\right)}{\partial y} \right) - \frac{1}{h_2}\frac{\partial v}{\partial x_1}\frac{\partial}{\partial y}\left(\frac{h_2}{h_1} \right) \right] + \mathcal{O}\left(\epsilon^3\right), \end{aligned} \tag{3.7}$$

where p is given by (3.4). The corresponding equation for u_2 is obtained similarly but is omitted here for brevity.

The first term of (3.7) in curly braces corresponds to the inertial terms, while the remaining terms on the left hand side correspond to the pressure and streamwise gravitational terms. The leading order term on the right hand side represents cross-stream friction, while the remaining terms correspond to additional viscous dissipation.

The final constraints are the tangential stress conditions (2.3) at the interface. Substitution of the Cauchy stress components (2.18)-(2.20) and the appropriate tan-

gent vectors (2.11) into (2.3) gives

(3.8)
$$\begin{aligned}0 = {} & \tilde{h}_2\left(\tilde{h}_1^2-\epsilon^2\eta_{x_1}^2\right)\left(\tilde{h}_1\frac{\partial}{\partial y}\left(\frac{u_1}{h_1}\right)\bigg|_\eta+\frac{\epsilon^2}{\tilde{h}_1}\frac{\partial v}{\partial x_1}\right)\\ & +\epsilon^2\left[2\tilde{h}_1\tilde{h}_2\eta_{x_1}\left(\frac{\partial v}{\partial y}-\frac{1}{\tilde{h}_1}\frac{\partial u_1}{\partial x_1}-\frac{u_2}{\tilde{h}_1\tilde{h}_2}\frac{\partial h_1}{\partial x_2}-\frac{v}{\tilde{h}_1}\frac{\partial h_1}{\partial y}\right)\right.\\ & \left.-\tilde{h}_1^2\eta_{x_2}\left(\frac{\tilde{h}_1}{\tilde{h}_2}\frac{\partial}{\partial x_2}\left(\frac{u_1}{h_1}\right)+\frac{\tilde{h}_2}{\tilde{h}_1}\frac{\partial}{\partial x_1}\left(\frac{u_2}{\tilde{h}_2}\right)\right)-\tilde{h}_1\tilde{h}_2\eta_{x_1}\eta_{x_2}\frac{\partial}{\partial y}\left(\frac{u_2}{h_2}\right)\right]\bigg|_\eta+\mathcal{O}\left(\epsilon^3\right),\end{aligned}$$

for the x_1 direction; the x_2 direction is again obtained similarly. (3.7) and (3.8) are original, and constitute the basis for many of the results in this paper.

3.2. Inertialess solution at $\mathcal{O}(\epsilon)$. First we consider the simplest case, which corresponds to many of the leading order solutions in the existing literature [15, 10, 32, 11]: we set $Re = 0$, and truncate the boundary layer equation (3.7) at $\mathcal{O}(\epsilon)$, giving

$$\frac{\epsilon}{h_1}\left(\frac{1}{Ca}\frac{\partial\kappa}{\partial x_1}-g_3\frac{\partial\eta}{\partial x_1}\right)+g_1=\frac{1}{h_2}\frac{\partial}{\partial y}\left(\frac{h_2}{h_1}\frac{\partial}{\partial y}\left(h_1u_1\right)\right)+\mathcal{O}\left(\epsilon^2\right). \tag{3.9}$$

This is to be solved subject to the no-slip and tangential stress conditions (3.8)

$$u_1|_{y=\zeta}=0,\quad \left(\tilde{h}_1\frac{\partial u_1}{\partial y}-u_1\frac{\partial h_1}{\partial y}\right)\bigg|_{y=\eta}=0+\mathcal{O}\left(\epsilon^2\right). \tag{3.10}$$

This gives

$$u_1=f_1^{(0)}g_1+\epsilon\left(\frac{1}{Ca}\frac{\partial\kappa}{\partial x_1}-g_3\frac{\partial\eta}{\partial x_1}\right)f_1^{(1)}+\mathcal{O}\left(\epsilon^2\right), \tag{3.11}$$

where

$$\begin{aligned}h_1f_1^{(0)} = {} & -\frac{1}{2k_2}\left(\frac{1}{2}y\left(h_1+\frac{m_1}{m_2}h_2\right)+\frac{1}{3}m_1k_1k_2y^3\right)\\ & +c_1^{(0)}\left(\frac{k_1k_2y+(k_1-k_2)\log h_2}{k_2^2}\right)+c_2^{(0)},\end{aligned} \tag{3.12}$$

$$\begin{aligned}h_1f_1^{(1)} = {} & -\frac{y}{k_1}+\frac{y^2}{2}+\frac{k_1-k_2}{k_1k_2}\left[y\left(1-\log\left(\frac{k_2}{k_2-k_1}\right)\right)\right.\\ & \left.+\frac{1-k_1y}{k_1}\log\left(1-k_1y\right)+\frac{(k_1-k_2)}{k_1k_2}\mathrm{Li}_2\left(\frac{k_1\left(1-k_2y\right)}{k_1-k_2}\right)\right]\\ & +c_1^{(1)}\frac{k_1k_2y+(k_1-k_2)\log h_2}{k_2^2}+c_2^{(1)}\end{aligned} \tag{3.13}$$

where $\mathrm{Li}_2(z)=-\int_0^z\frac{\log(1-t)}{t}dt$ is Jonquière's function of order 2 [25], and $c_{1,2}^{(0,1)}$ are constants of integration fixed by imposing (3.10); their evaluation is straightforward but cumbersome and so their general forms are omitted here.

3.3. Solution at higher orders. We now demonstrate how to extend the model to higher orders via a generalisation of the method of weighted residuals [40, 38]. We begin by considering (3.7) at leading order,

$$\frac{1}{h_2}\frac{\partial}{\partial y}\left(\frac{h_2}{h_1}\frac{\partial}{\partial y}\left(h_1 u_1\right)\right) = g_1 + \mathcal{O}\left(\epsilon\right), \tag{3.14}$$

whose solution is $u_1 = g_1 f_1^{(0)}$. We therefore consider a expansion of the form

$$u_1 = a_0(x_1, x_2, t) f_1^{(0)}(x_1, x_2, y) + \epsilon \sum_{i=1}^{N} a_i(x_1, x_2, t) b_i(y) + \mathcal{O}\left(\epsilon^2\right), \tag{3.15}$$

onto which we project. The procedure [38] is to then substitute this candidate velocity into (3.7), truncate at second order and integrate it together with an appropriate weight function $w\left(x_1, x_2, y\right)$ to determine evolution equations for the a_i. In order to facilitate this procedure, we first define the flux

$$q_1(x_1, x_2, t) = \int_{\zeta}^{\eta} h_2 u_1 dy. \tag{3.16}$$

Integrating (3.15) across the liquid layer and eliminating a_0 in favour of q_1 gives

$$u_1 = \frac{q_1 - \epsilon \sum\limits_{i=1}^{N} a_i \int_{\zeta}^{\eta} h_2 b_i dy + \mathcal{O}\left(\epsilon^2\right)}{\int_{\zeta}^{\eta} h_2 f_1^{(0)} dy} f_1^{(0)} + \epsilon \sum_{i=1}^{N} a_i b_i + \mathcal{O}\left(\epsilon^2\right). \tag{3.17}$$

As suggested by the kinematic condition, we use the inner product

$$\langle w, \cdot \rangle = \int_{\zeta}^{\eta} h_1 h_2 w \cdot dy. \tag{3.18}$$

In general, taking the inner product of w with the boundary layer equation (3.7) would require determination of b_i for $i \geq 1$. However, we show that careful selection of the weight w can avoid this cumbersome procedure [38].

Consider where terms involving a_i, $i \geq 1$ enter into the calculation. By (3.15) these are already of first order in ϵ. If they are substituted into second order viscous terms such as $\epsilon^2 \frac{\partial^2 u_1}{\partial x_i^2}$ (3.7) their contribution is of third order and thus negligible. In line with the simplified model [40], we also neglect their contributions to inertia where they would enter at second order. Thus the a_i, $i \geq 1$ enter only via the leading order cross-stream viscous term.

For the leading order cross-stream viscous term, we calculate directly by taking

the inner product of the weight w with the appropriate term in (3.7):

$$\begin{aligned}
&\left\langle w, \frac{1}{h_2}\frac{\partial}{\partial y}\left(\frac{h_2}{h_1}\frac{\partial}{\partial y}\left(h_1 u_1\right)\right)\right\rangle = \int_\zeta^\eta w h_1 h_2 \left[\frac{1}{h_2}\frac{\partial}{\partial y}\left(\frac{h_2}{h_1}\frac{\partial}{\partial y}\left(h_1 u_1\right)\right)\right] dy \\
&= \left[w h_2 \frac{\partial}{\partial y}\left(h_1 u_1\right)\right]_\zeta^\eta - \left[\frac{\partial}{\partial y}\left(w h_1\right) h_2 u_1\right]_\zeta^\eta + \int_\zeta^\eta h_1 u_1 \frac{\partial}{\partial y}\left(\frac{h_2}{h_1}\frac{\partial}{\partial y}\left(w h_1\right)\right) dy \\
&= -\overbrace{\left(w h_2 \frac{\partial}{\partial y}\left(h_1 u_1\right)\right)\Big|_{y=\zeta}}^{=I_1} + h_1 h_2 \overbrace{\left(w\frac{\partial u_1}{\partial y} - u_1 \frac{\partial w}{\partial y}\right)\Big|_{y=\eta}}^{=I_2} \\
&\qquad + \int_\zeta^\eta h_2 u_1 \overbrace{\frac{h_1}{h_2}\frac{\partial}{\partial y}\left(\frac{h_2}{h_1}\frac{\partial}{\partial y}\left(w h_1\right)\right)}^{=I_3} dy. \qquad (3.19)
\end{aligned}$$

where in deriving (3.19) we have made use of the no-slip condition (2.5) and integration by parts. Dependence on the a_i for $i \geq 1$ can be removed entirely, and the system made as simple as possible, as follows:

1. I_1 is best simplified by taking $w|_{y=\zeta} = 0$ in order to remove this term.
2. By comparison with the leading order contribution in (3.8), we wish I_2 to take the form $h_1 \frac{\partial u_1}{\partial y} - u_1 \frac{\partial h_1}{\partial y}$ so that this term introduces the relevant tangential stress term. I_2 is of this form if we take $\frac{w}{h_1} = \frac{\partial w/\partial y}{\partial h_1/\partial y}$, or equivalently, $h_1 \frac{\partial w}{\partial y} - w\frac{\partial h_1}{\partial y} = 0$.
3. I_3 is best simplified by taking $\frac{h_1}{h_2}\frac{\partial}{\partial y}\left(\frac{h_2}{h_1}\frac{\partial}{\partial y}\left(w h_1\right)\right) = 1$, so that the remaining integral is exactly $q_1 = \int_\zeta^\eta h_2 u_1 dy$.

Imposing these three constraints gives exactly

$$w = f_1^{(1)}, \qquad (3.20)$$

which is the function corresponding to the pressure term in (3.11). The constraints 1-3 above prescribing the weight w constitute the adjoint problem to that satisfied by the leading order velocity, as one would expect [39, 9, 30]. However, the viscous operator is not self-adjoint in the general case, and so the formulation is not Galerkin as seen in other applications of the method of weighted residuals [39, 38]. This calculation shows that nonetheless the weighted residual formulation can be extended into our general setting, regardless of the exact form of the substrate.

Ultimately we are projecting onto the single function $f_1^{(0)}$ (3.15) as the contributions of the additional terms b_i have been neglected. We have had success in gaining increased accuracy by extending our analyses by including higher order terms (up to fourth order) in the boundary layer equations, but still only projecting onto a single function, although these results are not presented here.

4. Recovery of existing models. The procedure outlined above recovers and indeed improves the majority of models in the literature. The exceptions largely consist of models that are inconsistent due to some *ad hoc* assumption, and the models of Ruyer-Quil & Manneville [38] that incorporate second order inertial effects. We give several examples here, although only §4.3 includes inertial effects.

4.1. Axisymmetric long-wave flow on a fibre. For flow down a vertical fibre we identify the co-ordinate x_1 with the axial direction z, and x_2 with the azimuthal

direction θ. Then for a cylinder of radius α the curvatures are $k_1 = 0$ and $k_2 = -1/\alpha$ while the substrate scale factors are $m_1 = 1$ and $m_2 = \alpha$. Then, taking $Ca = 1$ and taking gravity to be in the x_1 direction, (3.11) gives

$$u_1 = \frac{1}{4}\left(y(2\alpha + y) - 2(\alpha + \eta)^2 \log\left[1 + \frac{y}{\alpha}\right]\right)(1 - \kappa_z), \tag{4.1}$$

where suffices define appropriate partial derivatives. Substitution of this into (3.1) and redefining $\eta = S - \alpha$ (so that S is the radial position of the interface) to correspond with Craster & Matar [10] yields

$$8\left(S^2\right)_t = \frac{\partial}{\partial z}\left([\kappa_z - 1]\left[2S^2\left(\alpha^2 - S^2 + 2S^2 \log\frac{S}{\alpha}\right) - \left(\alpha^2 - S^2\right)^2\right]\right), \tag{4.2}$$

exactly as given by equation (2.17) in Craster & Matar [10]. Their choice of curvature κ is indeed an appropriate special case of (2.9). When the film is thin relative to the radius of curvature, (4.2) recovers the cylindrical model (2) of Roy et al., as detailed by Craster & Matar.

4.2. Nonaxisymmetric thin-film flow on a fibre. We now consider thin-film flow on a cylinder. In our system, that is equivalent to having a weak azimuthal curvature. Therefore we take the co-ordinate x_1 to be the axial direction z and the co-ordinate x_2 to be the azimuthal direction θ. Then the curvatures are $k_1 = 0$ and $k_2 = -\epsilon$ while the substrate scale factors are $m_1 = m_2 = 1/\epsilon$, and we obtain $h_1 = \epsilon^{-1}, \quad h_2 = \epsilon^{-1} + y$. As gravity is acting in the z direction, the expressions for the velocity (3.11) become

$$u_1 = \epsilon\left(\frac{y^2}{2} - \eta y\right)(\kappa_z - 1), \quad u_2 = \epsilon\left(\frac{y^2}{2} - \eta y\right)\kappa_\theta, \tag{4.3}$$

where $\kappa = -\eta - \nabla^2\eta$ is the appropriate expansion of (2.9). In this quasi-planar context, we have $\nabla = \begin{pmatrix}\partial_\theta \\ \partial_z\end{pmatrix}$, so that $\nabla^2 = \partial_\theta^2 + \partial_z^2$. Substitution into (3.1) and replacing η by h for comparison yields (2.15) in Wray et al. [53] for $\delta = 0$,

$$h_t + h^2 h_z + \frac{1}{3}\nabla \cdot \left(h^3 \nabla\left(h + \nabla^2 h\right)\right) = 0. \tag{4.4}$$

The second, third and fourth terms represent convective flow due to gravity, surface tension due to azimuthal curvature and surface tension due to axial curvature respectively.

4.3. Flow down a wavy inclined plane. We recover the model of Oron and Heining [32]: we consider flow down an undulating, inclined plane. So we are working in a planar situation, but with the substrate located at $y = \zeta(x_1)$. As the reference surface in this case is planar and one dimensional we ignore all contributions and derivatives in the x_2 direction, and take $m_1 = 1, \quad k_1 = 0$. We also drop the suffix 1.

We let $\chi = \eta - \zeta$ be the thickness of the flow at a given position. In order to match with [32] we take $g_3 = -B, g = 1$ and $Re = 1$ so that by (3.17) and (3.20),

$$u = \frac{q f_1^{(0)}}{\int_\zeta^\eta f_1^{(0)} dy} = -\frac{3q}{2\chi^3}\left((y - \eta)^2 - \chi^2\right), \quad w = \frac{1}{2}\left((y - \eta)^2 - \chi^2\right). \tag{4.5}$$

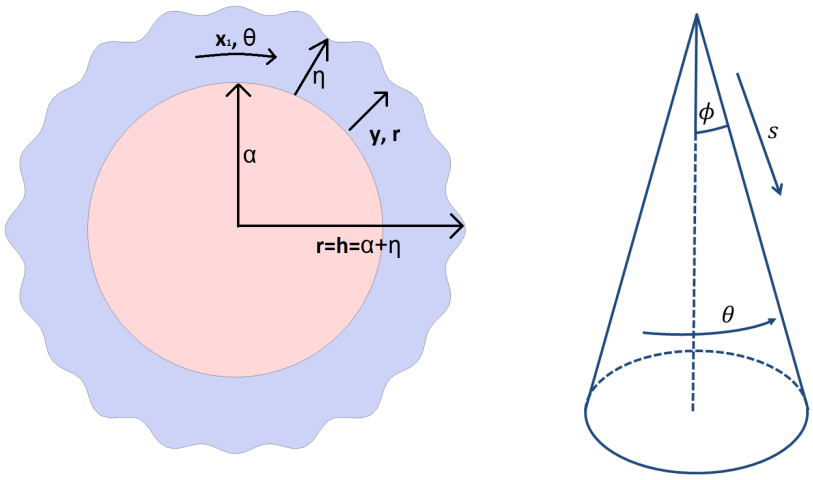

FIG. 2. *Schematics of example situations. Left: annular flow around a disc used in Sections 5 and 6. Right: conical substrate used in Section 7. Cone has apex angle 2ϕ. The co-ordinate s is the distance from the apex, and θ is the azimuthal angle. The substrate is at $y = 0$, and the normal is defined so that the fluid lies in the region $y > 0$ on the outside of the cone.*

We now substitute u into (3.7), multiply by w, integrating from ζ to η, set ϵ to unity and replace η with h to yield

$$h_t + q_x = 0, \quad q_t - \frac{9}{7}\frac{q^2\chi_x}{\chi^2} + \frac{17}{7}\frac{qq_x}{\chi} + \frac{5}{2}\frac{q}{\chi^2} = \left(1 - Bh_x + \frac{h_{xxx}}{Ca}\right)\frac{5}{6}\chi, \tag{4.6}$$

exactly as given in Oron & Heining [32].

This system does indeed preserve mass, and has the correct quasi-equilibrium solution $q \approx \chi^3/3$. However, it does omit Trouton viscosity terms that are found in other models [35] (58).

5. Example case 1: Thick annular flow at $Re = 0$. As a prototypical thick-film problem, we consider annular flow around a cylinder of radius α as shown on the left hand side of Figure 2, where we are neglecting variation in the axial direction so that $\frac{\partial}{\partial z} \equiv 0$. We assume that there is no gravity and that the flow is purely capillarity-driven; it is thus expected to be linearly stable. While simple, this demonstrates an important point: even in such an example, classical thin-film models exhibit margins of error in excess of 100% in certain parameter ranges. The model described in this paper is shown to perform better, opening up the opportunity for modelling thick liquid layers.

In the absence of gravity, the characteristic velocity must be re-defined as $U = \gamma/\mu$ as described in Section 2.1, so that $Ca = 1$. The leading order driving force is now the capillarity due to curvature gradients $\epsilon\partial_{x_i}\kappa$ rather than the gravity, and so we work relative to this as now being the leading order. For a cylinder of radius α

$$m_1 = \alpha; \quad k_1 = -1/\alpha; \quad m_2 = 1; \quad k_2 = 0, \tag{5.1}$$

and we assume $u_2 = 0$. We redefine our variables as

$$\alpha + y \mapsto r; \quad \alpha + \eta \mapsto h; \quad x_1 \mapsto \theta; \quad u_1 \mapsto u, \tag{5.2}$$

so that r is the radial spatial variable, and $h(\theta,t)$ is the radial location of the interface.

We calculate the exact linear stability in §5.1, the classical thin-film solution in §5.2, the leading order thick-film long-wave solution in §5.3.1 and the full second order thick-film long-wave solution in §5.3.2. The respective linear stabilities are compared in Section 5.4.

5.1. Exact linear stability. We introduce the stream function ξ so that $u = \frac{1}{r}\frac{\partial \xi}{\partial \theta}, \quad v = -\frac{\partial \xi}{\partial r}$. The system admits a basic solution $u = v = 0$, so that $\xi = 0$, with $h = \bar{h}$ being arbitrary. The basic value of the pressure p is then $p = \bar{p} = 1/\bar{h}$. We expand about this state using Fourier modes, so that $(\xi, p, h) = (0, \bar{p}, \bar{h}) + \delta e^{\sigma t + in\theta}(\psi(r), \tilde{p}(r), \tilde{h}(r))$, where $\delta \ll 1$, σ is the growth rate and n is the azimuthal wavenumber. Then elimination of pressure from the Navier-Stokes equations via cross differentiation gives ψ as satisfying the biharmonic equation in Fourier space

$$\frac{1}{r}\frac{d}{dr}\left(r\frac{d}{dr}\left(\frac{1}{r}\frac{d}{dr}\left(r\frac{d\psi}{dr}\right)\right)\right) - 2\frac{n^2}{r^2}\psi'' + \frac{n^4}{r^4}\psi + 2\frac{n^2}{r^3}\psi' - 4\frac{n^2}{r^4}\psi = 0. \tag{5.3}$$

This has general solution

$$\psi = Ar^{n+2} + Br^n + Cr^{2-n} + Dr^{-n}, \quad n \in \mathbb{Z} \setminus \{-1, 0, 1\}. \tag{5.4}$$

Thus there are 5 unknowns: $\{A, B, C, D, \tilde{h}\}$ that are determined using 5 constraints: no-slip and impermeability at the inner cylinder,

$$\psi_r|_{r=\alpha} = 0, \quad \psi_\theta|_{r=\alpha} = 0, \tag{5.5}$$

and the normal and tangential stress and kinematic conditions evaluated at the interface $r = h$, respectively,

$$\bar{h}^3\psi''' + \bar{h}^2\psi'' - \left(1 + 3n^2\right)\bar{h}\psi' + 4n^2\psi = in\left(1 - n^2\right)\tilde{h}, \tag{5.6}$$

$$\bar{h}^2\psi'' - \bar{h}\psi' + n^2\psi - \bar{h}\tilde{h}\bar{\xi}_{rr} = 0, \quad \tilde{h}s = \frac{in}{\bar{h}}\left(\tilde{\psi} + \bar{\xi}_r\tilde{h}\right). \tag{5.7}$$

Now, by substituting (5.4) into (5.5), (5.6) and (5.7), we eliminate A, B, C, D and $\tilde{h}$ in order to derive an equation for the growth rate σ:

$$\sigma = \frac{n\left(-\alpha^2\bar{h}^{4n+2} + \bar{h}^2\alpha^{4n+2} + n\left(\bar{h}^4 - \alpha^4\right)\bar{h}^{2n}\alpha^{2n}\right)}{2\bar{h}\left(\alpha^2\bar{h}^{4n+2} + \bar{h}^2\alpha^{4n+2} + \bar{h}^{2n}\alpha^{2n}\left(\bar{h}^4n^2 - 2\alpha^2\bar{h}^2\left(n^2-1\right) + \alpha^4n^2\right)\right)}. \tag{5.8}$$

5.2. Classical thin-film solution. Classical thin-film theory makes the substitution $\partial_r \mapsto \epsilon^{-1}\partial_r$. As shown by Wray et al. [52] the appropriate asymptotic scalings are $v = \epsilon^3 v_0$, $u = \epsilon^2 u_0$, $p = p_0$, $\partial_t \mapsto \epsilon^2\partial_t$. Then the leading order governing equations are

$$p_{0r} = 0, \quad \frac{1}{\alpha}p_{0\theta} = u_{0rr}, \quad 0 = v_{0r} + \frac{1}{\alpha}u_{0\theta}, \quad \kappa^{\mathrm{tf}} = \frac{1}{h} - h_{\theta\theta}, \quad p_0|_{r=h} = \kappa^{\mathrm{tf}}, \tag{5.9}$$

$$(u_{0r})|_{r=h} = 0, \quad u_0|_{r=\alpha} = 0, \quad v_0|_{r=\alpha} = 0, \quad \alpha h_t + \frac{\partial}{\partial\theta}\int_\alpha^h u\,dr = 0. \tag{5.10}$$

where κ^{tf} is the appropriate expansion of (2.9), including the regularising $h_{\theta\theta}$ term. This gives $v_0 = \left[\frac{r^2-\alpha^2}{2\alpha} + h\left(1-\frac{r}{\alpha}\right)\right]\kappa_\theta^{\text{tf}}$, and insertion into the kinematic condition provides

$$h_t = \left[\frac{(h-\alpha)^3}{3\alpha^2}\kappa_\theta^{\text{tf}}\right]_\theta. \tag{5.11}$$

This thin-film equation linearises as

$$\sigma = \frac{n^2\left(n^2-1\right)(\alpha-\bar{h})^3}{3\alpha^2\bar{h}^2}. \tag{5.12}$$

5.3. Long-wave solution. We now compute the long-wave solutions according to the method outlined in Section 3.3. In this geometry the curvature (2.9) becomes

$$\kappa = \frac{2h_\theta^2 + h\left(h - h_{\theta\theta}\right)}{\left(h^2+h_\theta^2\right)^{3/2}} \tag{5.13}$$

5.3.1. At first order. By (3.1) and (3.11)

$$\left(h^2\right)_t + \left[\frac{\kappa_\theta}{4\alpha^2}\left(\alpha^4 - h^4 + 4\alpha^2h^2\log\left(h/\alpha\right)\right)\right]_\theta = 0 + \mathcal{O}\left(\epsilon^2\right). \tag{5.14}$$

h^2 is a conserved quantity due to conservation of mass. Linearizing about $h = \bar{h}$ =const. and looking for solutions proportional to $e^{\sigma t+in\theta}$ gives

$$\sigma = \frac{n^2\left(n^2-1\right)\left(\alpha^4 - \bar{h}^4 + 4\alpha^2\bar{h}^2\log\left(\frac{\bar{h}}{\alpha}\right)\right)}{8\alpha^2\bar{h}^3}. \tag{5.15}$$

As validated in Section 5.4 this already outperforms classical thin-film theory as regards accuracy. However, the accuracy can again be improved significantly by extending it to an additional order as shown next.

5.3.2. At second order. As detailed in Section 3.3, we now proceed using the inner product and weight (3.18) and (3.20) respectively, which in this geometry become

$$\langle w, \cdot\rangle = \int_0^\eta rw\cdot dy, \quad w = \frac{r}{2}\log\frac{r}{\alpha} + h^2\frac{1}{4r\alpha^2}\left(\alpha^2-r^2\right). \tag{5.16}$$

As this flow is driven by a pressure gradient rather than gravity, per (3.11),

$$u = \frac{\kappa_\theta}{4r\alpha^2}\left(\left(\alpha^2-r^2\right)h^2 + 2r^2\alpha^2\log\left(r/\alpha\right)\right) \propto w. \tag{5.17}$$

Therefore we set

$$u = \frac{q(t,\theta)w(r,\theta) + \mathcal{O}\left(\epsilon\right)}{\phi}, \quad \phi = \int_\alpha^h r\,w\,dr = \frac{1}{8\alpha^2}\left(\alpha^2 - h^4 + 4\alpha^2h^2\log\frac{h}{\alpha}\right).$$

Now we compute the relevant inner product for each term in (3.7). The resultant expression is rather complex. But with ϵ set to unity, it is readily linearised as before to give

$$\sigma = \frac{3n^2(n^2-1)(\alpha^4-\bar{h}^4+4\alpha^2\bar{h}^2\log\frac{\bar{h}}{\alpha})^2}{2\bar{h}\left\{3(\alpha^4-\bar{h}^4)(4\alpha^2\bar{h}^2+n^2(\alpha^4+\bar{h}^4-6\alpha^2\bar{h}^2))+4\alpha^2\bar{h}^2\log\frac{\bar{h}}{\alpha}\times \left[12\alpha^2\bar{h}^2+3n^2(\alpha^4+\bar{h}^4-6\alpha^2\bar{h}^2)+n^2\log\frac{\bar{h}}{\alpha}(3\alpha^4-3\bar{h}^4+4\alpha^2\bar{h}^2\log\frac{\bar{h}}{\alpha})\right]\right\}}. \tag{5.18}$$

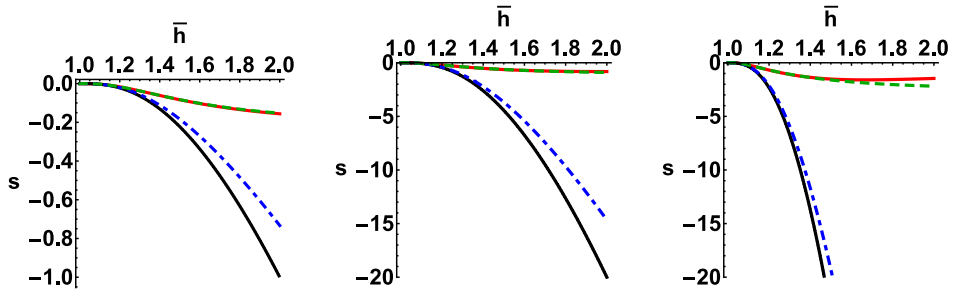

FIG. 3. *Plot of growth rate σ as a function of interfacial position $\bar{h}$ with $\alpha = 1$. Left: $n = 2$, middle: $n = 4$, right: $n = 6$. Solid red line: Exact Stokes solution, dashed green line: second order long-wave theory, dash-dotted blue line: first order long-wave theory, dotted black line: thin-film theory*

5.4. Comparison of linear theories. We have the linear stability as predicted by exact Stokes theory (5.8), thin-film theory (5.12) and long-wave theory at both first order (5.15) and second order (5.18). We have evaluated how well the theories perform for relatively thick films by examining the predictions of linear stability parametrically for $\alpha = 1$, $1 < \bar{h} < 2$ for wavenumbers $n = 2, 4$ and 6 in Figure 3. Even at leading order, long-wave theory (dash-dotted lines) gives somewhat better agreement than thin-film theory (dashed lines). We therefore recommend using this in circumstances where a simple first-order model is desired. More significantly, the second-order long-wave theory gives good results for thicker films than were previously accessible. For example for $n = 6$ and $\bar{h} = 1.5$ we find that thin-film theory predicts a growth rate of $\sigma = -23.3$, which is an error of over 1400% relative to the exact value of $\sigma = -1.517$. For comparison, the second-order model gives $\sigma = -1.607$, an error of less than 6%. When $\bar{h} = 2$, the thickness of the fluid is equal to the radius of the cylinder. We thus have a reduced model that performs well in analysing the behaviour of a thick liquid layer, at least in the stable, linear regime considered here.

6. Example case 2: Thick film hanging from a rotating cylinder at $Re = 0$. We now present a non-linear computation for the flow of a thick liquid layer hanging from a horizontal cylinder. The intention of this is three-fold: firstly to show that the accuracy of the formulation persists into the non-linear regime, secondly to demonstrate a situation which contains a natural instability unlike the previous example, and finally to show how we can extend beyond the formulation given in Section 3 (in particular, we choose to have a flow driven at leading order by a moving substrate rather than gravity). We therefore take

$$g_3 = -G\sin\theta, \quad g_1 = -G\cos\theta, \quad m_1 = \alpha, \quad k_1 = -1/\alpha, \quad \zeta = 0, \tag{6.1}$$

and drop the suffix 1. The no-slip condition becomes

$$u|_{y=0} = c_V\,. \tag{6.2}$$

We have conducted the following non-linear computations for comparison:

1. We have performed a direct numerical simulation of the two-dimensional Stokes equations.
2. In section 6.1 we perform a classical leading order thin-film calculation, to produce a governing evolution equation which we have solved numerically.

3. In section 6.2 we use the second order long-wave formulation presented in Section 3.3. The resultant evolution equations have been solved numerically.

Using the same substitutions as before (5.2), the Stokes equations (2.13) become

$$0 = -\frac{\partial p}{\partial r} + \frac{1}{r}\frac{\partial}{\partial r}\left(r\frac{\partial v}{\partial r}\right) + \frac{1}{r^2}\frac{\partial^2 v}{\partial \theta^2} - \frac{v}{r^2} - \frac{2}{r^2}\frac{\partial u}{\partial \theta} - G\sin\theta, \tag{6.3}$$

$$0 = -\frac{1}{r}\frac{\partial p}{\partial \theta} + \frac{1}{r}\frac{\partial}{\partial r}\left(r\frac{\partial u}{\partial r}\right) - \frac{u}{r^2} + \frac{1}{r^2}\frac{\partial^2 u}{\partial \theta^2} + \frac{2}{r^2}\frac{\partial v}{\partial \theta} - G\cos\theta, \tag{6.4}$$

$$0 = \frac{\partial (rv)}{\partial r} + \frac{\partial u}{\partial \theta}. \tag{6.5}$$

These are to be solved subject to no-slip and impermeability at the surface of the cylinder,

$$u|_{r=\alpha} = c_V, \quad v|_{r=\alpha} = 0, \tag{6.6}$$

the normal stress condition at the interface $r = h$,

$$\left(\frac{\kappa}{Ca} - p\right)\left(h^2 + h_\theta^2\right) = -2h^2 v_r - 2h_\theta\left(u - v_\theta - hu_r\right) - 2\frac{h_\theta^2}{h}\left(u_\theta + v\right), \tag{6.7}$$

and the tangential stress condition at the interface

$$2h_\theta\left(v_r - \frac{1}{h}\left(v + u_\theta\right)\right) + \left(1 - \frac{h_\theta^2}{h^2}\right)\left(hu_r - u + v_\theta\right) = 0. \tag{6.8}$$

Substituting (5.2) into the general kinematic equation (3.1) gives

$$hh_t + \frac{\partial}{\partial \theta}\int_\alpha^h u\, dr = 0. \tag{6.9}$$

6.1. Classical thin-film calculation. Upon making the same substitutions as in Section 5.2 the leading order governing equations in the classical thin-film case become

$$p_{0_r} = -G\sin\theta, \quad \frac{1}{\alpha}\frac{\partial p}{\partial \theta} = u_{0rr} - G\cos\theta, \quad \alpha v_{0_r} + u_{0\theta} = 0, \quad \kappa^{\mathrm{tf}} = \frac{1}{h} - h_{\theta\theta}, \tag{6.10}$$

$$p_0|_{r=h} = \frac{\kappa^{\mathrm{tf}}}{Ca}, \quad u_{0r}|_{r=\alpha} = 0, \quad u_0|_{r=\alpha} = c_V, \quad v_0|_{r=\alpha} = 0, \quad \alpha h_t + \frac{\partial}{\partial \theta}\int_\alpha^h u\, dr = 0. \tag{6.11}$$

Solving for the velocity u_0 and substituting this into the kinematic equation gives

$$u_0 = c_V + \left[\frac{r^2 - \alpha^2}{2\alpha} + h\left(1 - \frac{r}{\alpha}\right)\right]\left(\frac{\kappa^{\mathrm{tf}}}{Ca} + G\sin\theta\right)_\theta \implies \tag{6.12}$$

$$h_t = -\frac{c_V}{\alpha}h_\theta + \left[\frac{(h-\alpha)^3}{3\alpha^2}\left(\frac{\kappa^{\mathrm{tf}}}{Ca} + G\sin\theta\right)_\theta\right]_\theta. \tag{6.13}$$

This is essentially Moffatt's equation [29].

6.2. Long-wave calculation. The expression for the curvature κ is the same as in Section 5 (5.13). At leading order the flow is purely due to rotation induced by the substrate, rather than gravity or pressure gradients. As a result we need to derive an expression for u. The system is governed to leading order by

$$\frac{\partial}{\partial r}\left(\frac{1}{r}\frac{\partial}{\partial r}(ru)\right) = 0 + \mathcal{O}(\epsilon), \quad u|_{r=\alpha} = c_V, \quad (hu_r - u)|_{r=h} = 0 + \mathcal{O}(\epsilon^2). \tag{6.14}$$

This has solution $u = \frac{c_V}{\alpha} r$, so by (3.17) we use

$$u = \frac{q\, r}{\int_\alpha^h r\, dr} + \mathcal{O}(\epsilon^2) = \frac{2q}{h^2 - \alpha^2} r + \mathcal{O}(\epsilon^2). \tag{6.15}$$

where $q = \int_\alpha^h u\, dr$ is the flux, so that the kinematic condition (6.9) becomes

$$h h_t + \frac{\partial q}{\partial \theta} = 0. \tag{6.16}$$

Setting ϵ to unity and taking the inner product of the weight (5.16) with (3.7) yields

$$\begin{aligned}&\frac{\partial}{\partial \theta}\left[\frac{\kappa}{Ca} + Gh\sin\theta + 2\, v_r|_h + \frac{u_\theta|_h}{h} + \int^h \frac{2}{r^2}\frac{\partial u}{\partial \theta} dr\right]\int_\alpha^h w\, dr + \mathcal{O}(\epsilon^3) \\ &= \int_\alpha^h \frac{\partial}{\partial r}\left(\frac{1}{r}\frac{\partial}{\partial r}(ru)\right) rw\, dr + \int_\alpha^h rw\left(\frac{2}{r^2}\frac{\partial^2 u}{\partial \theta^2} + \frac{2}{r^2}\frac{\partial v}{\partial \theta} + \frac{1}{r}\frac{\partial}{\partial \theta}\int^r \frac{2}{r^2}\frac{\partial u}{\partial \theta} dr\right) dr.\end{aligned} \tag{6.17}$$

Thus the system is closed by the equation

$$\begin{aligned}&\frac{1}{8\alpha^2}\left(\alpha^2 - h^4 + 4\alpha^2 h^2 \log\frac{h}{\alpha}\right)\frac{\partial}{\partial \theta}\left[\frac{\kappa}{Ca} + Gh\sin\theta\right] = \\ &q + \frac{c_V}{2\alpha}\left(\alpha^2 - h^2\right) - \left(\frac{\left(\alpha^2 - h^2\right)^2\left(\alpha^2 + h^2\right) h_\theta}{2\alpha^2 h^3}\right)\left(\frac{q}{h^2 - \alpha^2}\right)_\theta \\ &+ \frac{1}{4}\left(\alpha^2 - h^2\right)\left(-2 + \frac{\alpha^2}{h^2} + \frac{h^2}{\alpha^2} + 2\left(\log\frac{h}{\alpha}\right)^2\right)\left(\frac{q}{h^2 - \alpha^2}\right)_{\theta\theta} + \mathcal{O}(\epsilon^3).\end{aligned} \tag{6.18}$$

There is no time derivative here: this equation simply provides an additional implicit relation between the interfacial position h and the flux q. In absence of inertia q is still effectively slaved to h and thus does not have an independent evolution equation.

6.3. Numerical results. We now compare the nonlinear predictions of classical thin-film theory (6.13), the new long-wave theory (6.16) and (6.18), and direct numerical computations of (6.3)-(6.5). The direct numerical computations have been performed by rescaling onto a rectangular domain via the substitution $Y = (r-\alpha)/(h-\alpha)$, and using second-order centred finite differences in space and the second-order implicit trapezoidal rule in time. Grid size and time steps were both reduced until convergence was attained.

We find that for moderate values of c_V the system settles to a steady state. For $0.2 < c_V < 1$ we monitor $h_{\max}$, the maximum value of h at this steady state, and $\theta_{\max}$, the position of this maximum. We plot these as a function of c_V for direct

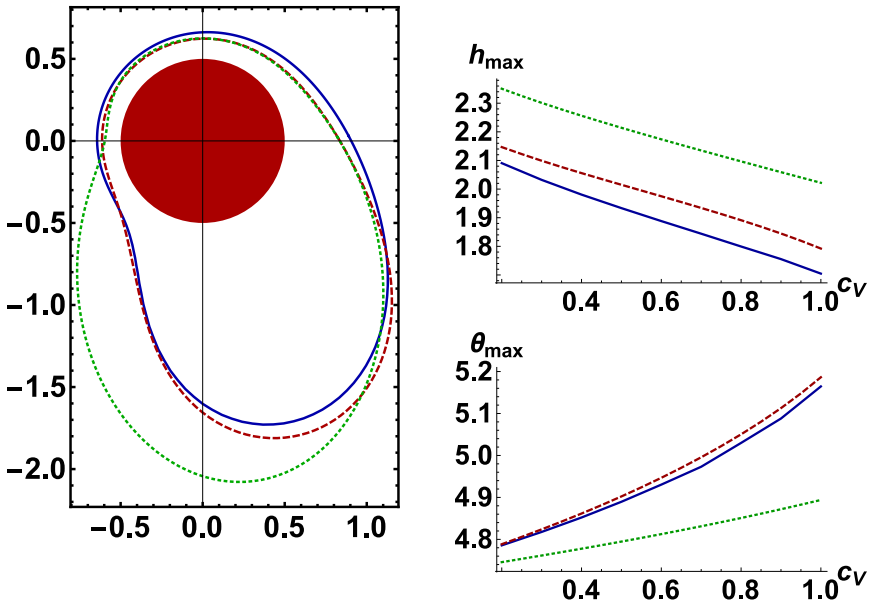

FIG. 4. *In all images the solid blue line corresponds to direct numerical simulation of the Stokes equations, the dashed red line to the long-wave model* (6.16), (6.18) *and the dotted green line to the thin-film model* (6.13). *Left: comparison of predicted droplet shapes at steady state for* $\bar{h} = 1, c_V = 0.8, \alpha = 0.5, Ca = 0.2$*; right, top and bottom: Plots of maximal film thickness at steady state* h_{max} *and position of this maximum* θ_{max} *for a variety of values of* c_V *with* $Ca = 0.2$, $\alpha = 0.5$, $G = 5$.

numerical simulations of the Stokes equations, for the thin-film model (6.13) and the long-wave model (6.16), (6.18) in Figure 4. As seen in the image on the left, thin-film theory conspicuously fails to preserve mass (as might be expected from the form of the kinematic equation (6.13) which preserves $\int h d\theta$, not $\int h^2 d\theta$; this happens precisely because the thin-film model neglects the details of geometric effects). The agreement between the long-wave theory and the Stokes equations is strong: the predicted value for $h_{\max}$ is in error by at most 5% in the given range, while $\theta_{\max}$ is never in error by more than 0.025 radians $\approx 1.5^{\circ}$. The thin-film model performs less well: the prediction for $h_{\max}$ is in error by as much as 18% for $c_V = 1$. In addition, the prediction for $\theta_{\max}$ is in error by as much as 0.22 radians $\approx 12.6^{\circ}$.

7. Example case 3: axisymmetric droplets on a cone at $Re = 0$**.** We now examine the case of a axisymmetric droplet ring on the surface of a cone. The predominant aim of this is to show how easy it is to produce a good model in a novel geometry. However, it also serves to again show the increased accuracy provided by this long-wave model. The co-ordinate system used on the underlying conical substrate is shown on the right hand side of Figure 2. This is essentially working in a polar co-ordinate system where the polar angle is fixed at ϕ as used in other studies [1, 14, 43].

The surface of the cone is located at $(X_1, X_2, X_3) = (s\sin\phi\cos\theta, s\sin\phi\sin\theta, s\cos\phi)$ so that

$$m_\theta = s\sin\phi, \quad m_s = 1, \quad k_\theta = -\cos\phi, \quad k_s = 0, \tag{7.1}$$

and thus

$$h_\theta = s\sin\phi\,(1+y\cos\phi)\,, \quad h_2 = 1. \tag{7.2}$$

Instead of working directly in the normal co-ordinate y, we make the substitution $r = \sin\phi\,(1+y\cos\phi)$. Now the lower wall is located at $r|_{y=0} = \sin\phi = \alpha$. These can be understood physically by considering sr which is the radial distance from the axis of the cone, and $s\alpha$ which is the radial distance of the substrate from the axis of the cone. The velocity in the s direction is denoted by u, and that in the wall-normal direction by v.

7.1. Stokes equations. In this geometry, the momentum equations in the s and y directions, and the continuity equation are given respectively by,

$$\frac{\partial p}{\partial s} - \cos\phi = \frac{\sin^2(2\phi)}{4r}\frac{\partial}{\partial r}\left(r\frac{\partial u}{\partial r}\right) + \frac{1}{s}\frac{\partial^2}{\partial s^2}(su) + \frac{1}{s}\frac{\partial v}{\partial s}, \tag{7.3}$$

$$\frac{\sin(2\phi)}{2}\frac{\partial p}{\partial r} + \sin\phi = \frac{\sin^2(2\phi)}{4r}\frac{\partial^2}{\partial r^2}(rv) + \frac{1}{s}\frac{\partial}{\partial s}\left(s\frac{\partial v}{\partial s}\right) + \frac{\sin(2\phi)}{2}\frac{\partial}{\partial s}(su)\,, \tag{7.4}$$

$$0 = \frac{\partial}{\partial s}(sru) + \frac{\sin(2\phi)}{2}\frac{\partial}{\partial r}(srv)\,. \tag{7.5}$$

These are to be solved subject to the no-slip and impenetrability conditions $u|_{r=\alpha} = v|_{r=\alpha} = 0$. The system is closed by the normal and tangential stress balances at the interface $r|_{y=\eta} = \sin\phi\,(1+\eta\cos\phi) = \Gamma$,

$$0 = \left(1-\eta_s^2\right)\left(\frac{\partial v}{\partial s} + \frac{\sin(2\phi)}{2}\frac{\partial u}{\partial r}\right) + 2\eta_s\left(\frac{\sin(2\phi)}{2}\frac{\partial v}{\partial r} - \frac{\partial u}{\partial s}\right), \tag{7.6}$$

$$p - \frac{\kappa}{Ca} = \frac{2}{1+\eta_s^2}\left(\frac{\sin(2\phi)}{2}\frac{\partial u}{\partial r} - \frac{\partial \eta}{\partial s}\left(\frac{\partial v}{\partial s} + \frac{\sin(2\phi)}{2}\frac{\partial u}{\partial r}\right) + \eta_s^2\frac{\partial u}{\partial s}\right), \tag{7.7}$$

where $\eta_s = \frac{2\Gamma_s}{\sin(2\phi)}$, and the kinematic condition at the interface is

$$\frac{\partial \Gamma}{\partial t} = \frac{\sin(2\phi)}{2}v - u\frac{\partial \Gamma}{\partial s} \implies s\Gamma\frac{\partial \Gamma}{\partial t} + \frac{\partial}{\partial s}\left(\int_\alpha^\Gamma sr\,u\,dr\right) = 0. \tag{7.8}$$

7.2. Reduced models. A similar procedure to that followed in Section 6.1 gives the thin-film equation as being

$$s\frac{\partial \Gamma}{\partial t} = \frac{\partial}{\partial s}\left[\frac{4s}{\sin^2(2\phi)}\frac{(\Gamma-\alpha)^2}{3}\left(\frac{\kappa_s}{Ca} + \frac{1}{\cos\phi}\Gamma_s - \cos\phi\right)\right], \tag{7.9}$$

where the appropriate expansion of the curvature term κ is

$$\kappa = \frac{\sin(2\phi)}{2\alpha} - \left[\frac{\sin(2\phi)}{2\alpha^2}\Gamma + \frac{2}{\sin(2\phi)}\frac{\Gamma_s}{s} + \frac{2}{\sin(2\phi)}\Gamma_{ss}\right] + \mathcal{O}\left(\epsilon^3\right). \tag{7.10}$$

The leading order long-wave solution becomes

$$s\Gamma\frac{\partial \Gamma}{\partial t} + \frac{\partial}{\partial s}\left(\frac{s}{4\sin^2(2\phi)}\left[\frac{\kappa_s}{Ca} + \frac{1}{\cos\phi}\Gamma_s - \cos\phi\right]\left[\alpha^4 - 4\alpha^2\Gamma^2 + 3\Gamma^4 - 4\Gamma^2\log\frac{\Gamma}{\alpha}\right]\right) + \mathcal{O}\left(\epsilon^2\right), \tag{7.11}$$

while the weight (3.20) is

$$w = \frac{1}{4}\left(r^2 - \alpha^2 - 2\Gamma^2 \log\frac{r}{\alpha}\right). \tag{7.12}$$

Taking the inner product of (3.7) with the weight (7.12) and setting ϵ to unity gives

$$\begin{aligned} 0 = {} & \frac{\sin^2(2\phi)}{4}\left(q_s + \frac{s\Gamma}{4}\left(\Gamma^2 - \alpha^2 - 2\Gamma^2\log\frac{\Gamma}{\alpha}\right)\left.\frac{\partial u}{\partial r}\right|_\Gamma\right) \\ & + \left[\cos\phi - \frac{1}{\cos\phi}\Gamma_s - \frac{\kappa_s}{Ca}\right]\left[\frac{s}{16}\left(\alpha^4 - 4\alpha^2\Gamma^2 + 3\Gamma^4 - 4\Gamma^4\log\frac{\Gamma}{\alpha}\right)\right] \\ & + \int_\alpha^\Gamma rsw\left[\frac{1}{s}\frac{\partial^2}{\partial s^2}(su) + \frac{1}{s}\frac{\partial v}{\partial s}\right]dr \\ & - \int_\alpha^\Gamma rsw\frac{\partial}{\partial s}\left\{\sin(2\phi)\left.\frac{\partial v}{\partial r}\right|_\Gamma + \left[\frac{\sin(2\phi)}{2}\frac{1}{r}\frac{\partial(rv)}{\partial r}\right]_r^\Gamma\right\}dr + \mathcal{O}\left(\epsilon^3\right), \end{aligned} \tag{7.13}$$

which is the full expression for the second order long-wave model.

7.3. Results. Similarly to Section 6, the results of the thin-film model (7.9), the first order long-wave model (7.11) and the full second order long-wave model (7.13) have been compared to direct numerical simulations of the Stokes equations (7.3) - (7.5).

We began by considering the flow of a drop deposited on a cone covered with a thin precursor film over a long period of time. We took $\phi = \pi/4$ and $Ca = 1$. We used an initial condition of $\eta = 0.1 + \exp\left(-(x-6)^2\right)$ and let the droplets evolve down the surface of the cone. In order to compare the accuracy of the results we considered an integral measure of error over the complete domain $\mathrm{e_{int}} = \int |\Gamma_{\mathrm{sim}} - \Gamma_{\mathrm{DNS}}|\, ds$, where Γ_{sim} are the results of the respective simulation and Γ_{DNS} is the result of the DNS calculation. The result of the DNS simulation is plotted as a surface of revolution about the axis of the cone at the top of Figure 5. The time evolution of the error is plotted in the bottom-left of Figure 5. As expected, the full long-wave model far outperforms both the other models, while the first order long-wave model still significantly improves on the predictions of the thin-film model.

Finally, we validated the interesting result that, under appropriate conditions, a droplet can be pulled up the surface of the cone by the effect of surface tension that has previously been observed experimentally in a similar context [26]. We therefore neglected the gravitational effects (which act to counter this) and set $\phi = 9\pi/20$ and $Ca = 0.01$. We then simulate over time and plot $\mathrm{s_{max}}$, the position of the highest point of the drop, in the bottom right of Figure 5. The droplet is indeed pulled up the surface of the cone (i.e. the distance down the cone $s_{\max}$ is decreasing), although the effect is small.

8. Conclusions. A novel formulation has been given for the flow of a thick film over an arbitrary, potentially highly undulatory surface. The flexibility of the system has been demonstrated by recovering a number of existing models in the literature, before being applied to derive and study several new models.

Firstly, this formulation extends previous work in general geometries by combining both a co-ordinate system body-fitted to a reference surface together with a spatially varying substrate position to overcome limitations inherent in existing formulations. As a result we can access a variety of situations that are not accessible by Roberts

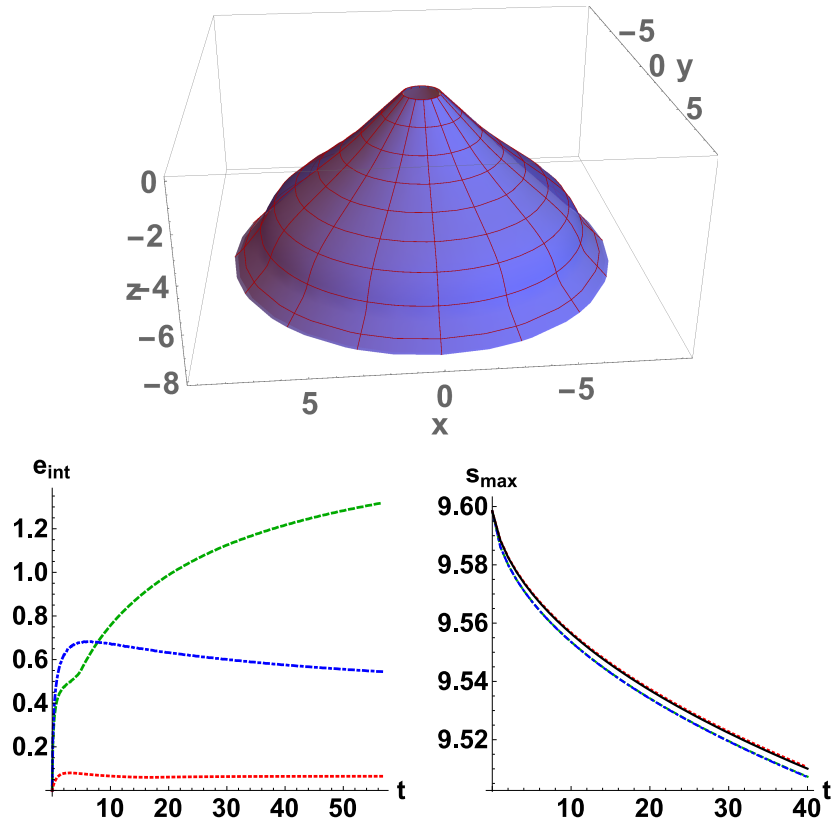

FIG. 5. *Top: Example of a flow on the surface of a cone. Bottom left: the error e_{int} as a function of time for each of the thin film (green, dashed), first order long-wave (blue, dash-dotted) and full long-wave (red, dotted) equations as a function of time when $\phi = \pi/4$ and $Ca = 1$. Bottom right: position of the peak of the droplet as a function of time when $\phi = 9\pi/20$ and $Ca = 0.01$, and we ignore gravitational effects. The results of direct numerical simulation are in black.*

& Li [35], Roy et al. [37] or Oron et al. [32]. In the future we plan to investigate whether other situations have been rendered accessible, such as flow on the outside of a sharply corrugated cylinder.

Secondly, by taking a less restrictive set of asymptotic scalings than those used by Roy et al. [37] we have broadened the applicability of our equations. This has resulted in better agreement with certain models in the literature that do consider highly curved substrates, such as those of Craster & Matar [10] and Ruyer-Quil et al. [39].

We have demonstrated that in the case of two dimensional annular flow, this second order separation of variables approach performs better than the classical leading order expansion approach that has been used extensively in the literature. We have shown that in the nonlinear regime the present approach can provide good agreement with the results of direct numerical computations. We have also shown that this agreement extends into more complicated geometries such as the motion of droplets on the surface on a cone. This has allowed for the computation of phenomena such as the surface tension driven motion of these droplets towards the cone tip as previously observed experimentally [26].

Future work will center on the use of models to access complex phenomena including additive surfactants and electric fields. Extensive studies are possible because the models can be solved numerically at speeds that are orders of magnitude faster than direct numerical simulations.

All three authors acknowledge the support of the EPSRC via grants EP/K041134/1, EP/L020564/1 and EP/K003976/1.

REFERENCES

[1] R. C. Ackerberg, *The viscous incompressible flow inside a cone*, J. Fluid Mech., 21 (1965), pp. 47–81.
[2] C. Ancey, *Plasticity and geophysical flows: A review*, J. Non-Newton. Fluid Mech., 142 (2007), pp. 4–35.
[3] D. R. Baral, K. Hutter, and R. Greve, *Asymptotic theories of large-scale motion, temperature, and moisture distribution in land-based polythermal ice sheets: A critical review and new developments*, Appl. Mech. Rev., 54 (2001), pp. 215–256.
[4] T. B. Benjamin, *Wave formation in laminar flow down an inclined plane*, J. Fluid Mech., 2 (1957), pp. 554–573.
[5] D. J. Benney, *Long waves on liquid films*, J. Math. and Phys., 45 (1966), pp. 150–155.
[6] R. J. Braun and A. D. Fitt, *Modelling drainage of the precorneal tear film after a blink*, Math. Med. Biol., 20 (2003), pp. 1–28.
[7] M. Cachile, M. A. Aguirre, M. Lenschen, and A. Calvo, *Flow of a thin liquid film coating a horizontal stationary cylinder*, Phys. Rev. E, 88 (2013), 063005.
[8] H.-C. Chang, *Wave evolution on a falling film*, Annu. Rev. Fluid Mech., 26 (1994), pp. 103–136.
[9] P. H. Coullet and E. A. Spiegel, *Amplitude equations for systems with competing instabilities*, SIAM J. Appl. Math., 43 (1983), pp. 776–821.
[10] R. V. Craster and O. K. Matar, *On viscous beads flowing down a vertical fibre*, J. Fluid Mech., 553 (2006), pp. 85–105.
[11] ———, *Dynamics and stability of thin liquid films*, Rev. Mod. Phys., 81 (2009), pp. 1131–1198.
[12] R. D. Deegan, O. Bakajin, T. F. Dupont, G. Huber, S. R. Nagel, and T. A. Witten, *Capillary flow as the cause of ring stains from dried liquid drops*, Nature, 389 (1997), pp. 827–829.
[13] J. C. T. Eijkel and A. van den Berg, *Nanofluidics: What is it and what can we expect from it?*, Microfluid. Nanofluid., 1 (2005), pp. 249–267.
[14] J. P. Fohr and J. Mallet, *Ecoulement visqueux entre deux cones coaxiaux*, Appl. Sci. Res., 30 (1975), pp. 221–236.
[15] P. S. Hammond, *Nonlinear adjustment of a thin annular film of viscous fluid surrounding a thread of another within a circular cylindrical pipe*, J. Fluid Mech., 137 (1983), pp. 363–384.
[16] C. Heining, V. Bontozoglou, N. Aksel, and A. Wierschem, *Nonlinear resonance in viscous films on inclined wavy planes*, Int. J. Multiph. Flow, 35 (2009), pp. 78–90.
[17] P. D. Howell, *Models for thin viscous sheets*, European J. Appl. Math., 7 (1996), pp. 321–343.
[18] ———, *Surface-tension-driven flow on a moving curved surface*, J. Engrg. Math., 45 (2003), pp. 283–308.
[19] H. E. Huppert, *The propagation of two-dimensional and axisymmetric viscous gravity currents over a rigid horizontal surface*, J. Fluid Mech., 121 (1982), pp. 43–58.
[20] H. E. Huppert and J. E. Simpson, *The slumping of gravity currents*, J. Fluid Mech., 99 (1980), pp. 785–799.
[21] S. Kalliadasis and H.-C. Chang, *Drop formation during coating of vertical fibres*, J. Fluid Mech., 261 (1994), pp. 135–168.
[22] S. Kalliadasis, C. Ruyer-Quil, B. Scheid, and M. G. Velarde, *Falling Liquid Films*, vol. 176 of Appl. Math. Sci., Springer, London, 2012.
[23] P. L. Kapitza and S. P. Kapitza, *Wave flow of thin layers of a viscous fluid*, Zh. Eksp. Teor. Fiz, 19 (1949), pp. 105–120.
[24] I. L. Kliakhandler, S. H. Davis, and S. G. Bankoff, *Viscous beads on vertical fibre*, J. Fluid Mech., 429 (2001), pp. 381–390.
[25] L. Lewin, *Polylogarithms and associated functions*, North-Holland, New York, 1981.
[26] É. Lorenceau and D. Quéré, *Drops on a conical wire*, J. Fluid Mech., 510 (2004), pp. 29–45.

[27] M. J. Miksis and M. P. Ida, *The dynamics of thin films I: General theory*, SIAM J. Appl. Math., 58 (1998), pp. 456–473.
[28] ———, *The dynamics of thin films II: Applications*, SIAM J. Appl. Math., 58 (1998), pp. 474–500.
[29] H. K. Moffatt, *Behaviour of a viscous film on the outer surface of a rotating cylinder*, J. Mécanique, 16 (1977), pp. 651–673.
[30] A. H. Nayfeh, *Resolving controversies in the application of the method of multiple scales and the generalized method of averaging*, Nonlinear Dynam., 40 (2005), pp. 61–102.
[31] A. Oron, S. H. Davis, and S. G. Bankoff, *Long-scale evolution of thin liquid films*, Rev. Mod. Phys., 69 (1997), pp. 931–980.
[32] A. Oron and C. Heining, *Weighted-residual integral boundary-layer model for the nonlinear dynamics of thin liquid films falling on an undulating vertical wall*, Phys. Fluids, 20 (2008), 082102.
[33] A. Pumir, P. Manneville, and Y. Pomeau, *On solitary waves running down an inclined plane*, J. Fluid Mech., 135 (1983), pp. 27–50.
[34] N. M. Ribe, *Bending and stretching of thin viscous sheets*, J. Fluid Mech., 433 (2001), pp. 135–160.
[35] A. J. Roberts and Z. Li, *An accurate and comprehensive model of thin fluid flows with inertia on curved substrates*, J. Fluid Mech., 553 (2006), pp. 33–73.
[36] P. Rosenau, A. Oron, and J. M. Hyman, *Bounded and unbounded patterns of the benney equation*, Phys. Fluids A, 4 (1992), pp. 1102–1104.
[37] R. V. Roy, A. J. Roberts, and M. E. Simpson, *A lubrication model of coating flows over a curved substrate in space*, J. Fluid Mech., 454 (2002), pp. 235–261.
[38] C. Ruyer-Quil and P. Manneville, *Improved modeling of flows down inclined planes*, Eur. Phys. J. B, 15 (2000), pp. 357–369.
[39] C. Ruyer-Quil, P. Treveleyan, F. Giorgiutti-Dauphiné, C. Duprat, and S. Kalliadasis, *Modelling film flows down a fibre*, J. Fluid Mech., 603 (2008), pp. 431–462.
[40] B. Scheid, C. Ruyer-Quil, and P. Manneville, *Wave patterns in film flows: Modelling and three-dimensional waves*, J. Fluid Mech., 562 (2006), pp. 183–222.
[41] B. Scheid, C. Ruyer-Quil, U. Thiele, O. A. Kabov, J. C. Legros, and P. Colinet, *Validity domain of the benney equation including the marangoni effect for closed and open flows*, Journal of Fluid Mechanics, 527 (2005), pp. 303–335.
[42] M. Scholle, A. Haas, N. Aksel, M. C. T. Wilson, H. M. Thompson, and P. H. Gaskell, *Competing geometric and inertial effects on local flow structure in thick gravity-driven fluid films*, Phys. Fluids, 20 (2008), 123101.
[43] M. A. Serag-Eldin and Y. K. Gayed, *Asymptotic solution of the low reynolds-number flow between two co-axial cones of common apex*, Int. J. Math. Math. Sci., 7 (1984), pp. 765–784.
[44] A. Sharma and E. Ruckenstein, *An analytical nonlinear theory of thin film rupture and its application to wetting films*, J. Coll. Int. Sci., 113 (1986), pp. 456–479.
[45] V. Y. Shkadov, *Wave flow regimes of a thin layer of viscous fluid subject to gravity*, Fluid Dyn., 2 (1967), pp. 29–34.
[46] G. I. Sivashinsky and D. M. Michelson, *On irregular wavy flow of a liquid film down a vertical plane*, Progr. Theoret. Phys., 63 (1980), pp. 2112–2114.
[47] T. M. Squires and S. R. Quake, *Microfluidics: Fluid physics at the nanoliter scale*, Rev. Modern Phys., 77 (2005), pp. 977–1026.
[48] H. A. Stone, A. D. Stroock, and A. Ajdari, *Engineering flows in small devices: microfluidics toward a lab-on-a-chip*, Annu. Rev. Fluid Mech., 36 (2004), pp. 381–411.
[49] A. Wierschem and N. Aksel, *Influence of inertia on eddies created in films creeping over strongly undulated substrates*, Phys. Fluids, 16 (2004), pp. 4566–4574.
[50] A. Wierschem, C. Lepski, and N. Aksel, *Effect of long undulated bottoms on thin gravity-driven films*, Acta Mech., 179 (2005), pp. 41–66.
[51] H Wong, I Fatt, and C J Radke, *Deposition and thinning of the human tear film*, J. Coll. Interface Sci., 184 (1996), pp. 44–51.
[52] A. W. Wray, O. K. Matar, and D. T. Papageorgiou, *Non-linear waves in electrified viscous film flow down a vertical cylinder*, IMA J. Appl. Math., 77 (2012), pp. 430–440.
[53] A. W. Wray, D. T. Papageorgiou, and O. K. Matar, *Electrostatically controlled large-amplitude, non-axisymmetric waves in thin film flows down a cylinder*, J. Fluid Mech., 736 (2013), R2.
[54] C.-S. Yih, *Stability of liquid flow down an inclined plane*, Phys. Fluids, 6 (1963), pp. 321–334.